Electrical & Computer Engineering Faculty Publications

Electrical & Computer Engineering

2012

Fast Stochastic Wiener Filter for Super-Resolution Image Restoration with Information Theoretic Visual Quality Assessment

Amr Hussein Yousef
Old Dominion University

Jiang Li
Old Dominion University, jli@odu.edu

Mohammad Karim
Old Dominion University

Mark Allen Neifeld (Ed.)

Amit Ashok (Ed.)

Follow this and additional works at: https://digitalcommons.odu.edu/ece_fac_pubs

Part of the Aviation Safety and Security Commons, Bioimaging and Biomedical Optics Commons, Electrical and Computer Engineering Commons, and the Theory and Algorithms Commons

Fast stochastic Wiener filter for Super-resolution Image Restoration with Information Theoretic Visual Quality Assessment

Amr Hussein Yousef, Jiang Li and Mohammad Karim

Department of Electrical and Computer Engineering

Old Dominion University, Norfolk, VA 23529

ABSTRACT

Super-resolution (SR) refers to reconstructing a single high resolution (HR) image from a set of subsampled, blurred and noisy low resolution (LR) images. The reconstructed image suffers from degradations such as blur, aliasing, photo-detector noise and registration and fusion error. Wiener filter can be used to remove artifacts and enhance the visual quality of the reconstructed images. In this paper, we introduce a new fast stochastic Wiener filter for SR reconstruction and restoration that can be implemented efficiently in the frequency domain. Our derivation depends on the continuous-discrete-continuous (CDC) model that represents most of the degradations encountered during the image-gathering and image-display processes. We incorporate a new parameter that accounts for LR images registration and fusion errors. Also, we speeded up the performance of the filter by constraining it to work on small patches of the images. Beside this, we introduce two figures of merits: information rate and maximum realizable fidelity, which can be used to assess the visual quality of the resultant images. Simulations and experimental results demonstrate that the derived Wiener filter that can be implemented efficiently in the frequency domain can reduce aliasing, blurring, and noise and result in a sharper reconstructed image. Also, Quantitative assessment using the proposed figures coincides with the visual qualitative assessment. Finally, we evaluate our filter against other SR techniques and its results were very competitive.

1. INTRODUCTION

Most SR approaches consist of three main steps: registration, reconstruction and restoration. Registration is a process of aligning several images to a reference one. Registration with subpixel accuracy is essential in reconstructing high resolution (HR) images with enhanced visual quality and minimum unwanted artifacts.[1] The subpixel registration techniques can be classified into four types: (1) Correlation interpolation, (2) Intensity interpolation, (3) Differential interpolation, and (4) Phase correlation.

Image reconstruction is a method of reconstructing HR images by incorporating the available different registered LR pixels to estimate the missing pixels on the HR grid. In most cases, the registered LR pixels are irregularly distributed over the HR grid. Popular techniques for image reconstruction[2] are nearest neighbor interpolation, bilinear interpolation, cubic spline interpolation and piecewise cubic convolution.[3] Image restoration is a method of correcting the reconstructed HR image from degraded LR images with blurring, aliasing and noise.[4] Popular restoration methods are inverse filters, least square filters, and iterative approaches.[2,5]

SR algorithms can be divided into two categories: spatial domain approaches and spatial frequency domain approaches.[1] Frequency domain approaches include reconstruction via aliasing removal, recursive least squares filters and multichannel sampling theorem based techniques.[1] Spatial domain approaches include non-uniform interpolation, algebraic filtered back projection, probabilistic methods like maximum likelihood (ML) estimation and maximum a posteriori (MAP) based algorithms, projection onto convex set (POCS), hybrid ML/MAP/POCS methods and Tikhonov-Arsenin regularized methods.[1] Frequency domain approaches are simple because the relation between the LR images and the HR images is easy to understand in the frequency domain. Also, they

have low computational complexity but their performance degrades if the motion model is other than a global translation and the blur kernel is not a linear shift invariant (LSI) one. On the other hand, spatial domain approaches can be exploited to work on any arbitrary motion and degradation models such as motion blur, spatially varying or invariant blur but they are computationally intensive approaches.[6]

In this paper, we propose A new fast optimal stochastic minimum square restoration Wiener filter for SR reconstruction and restoration is introduced. This filter is used to boost The visual quality of the SR image that is affected by degradations during the acquisition such as blur due to system optics, aliasing due to insufficient sampling, photodetector noise, registration and fusion error, the number of scenels, i.e., the number of overlapped images used for SR reconstruction within the HR grid and their relative arrangement on the high resolution grid. We formulate the Wiener filter as a function of the parameters associated with the proposed SR system such as image gathering and image display response indices, system average signal-to-noise ratio (SNR) and inter-subpixel shifts between the LR images. A new parameter that accounts for LR images registration and fusion errors is added to the SR CDC model in order to improve the overall system fidelity. In addition, The filter performance is speeded up by constraining it to work on small patches of the images and can be implemented efficiently in the frequency domain. Finally, to assess the visual quality of the resultant images, two figures of merits are introduced: information rate, and maximum realizable fidelity. Simulation results and quantitative assessments demonstrate that the speeded-up improved Wiener filter can reduce aliasing and blurring, resulting in a sharper reconstructed image with maximum realizable fidelity.

The rest of the paper is organized as follows. In Section 2, a quick review of the derivation of the stochastic Wiener restoration filter is presented. The enhancement of the end-to-end system fidelity is proposed in Section 3. In section 4, the speeding-up of the system performance is discussed and in Section 5 we assess the visual quality of the images based on information theory. We present our simulations and results in Section 5 and we conclude our work in Section 7.

2. DERIVED STOCHASTIC WIENER RESTORATION FILTER

Figure 1 details our Super-resolution CDC based system components. It represents most of the degradations including blur, noise and aliasing that are encountered during the image gathering, image reconstruction and image display processes. According to Carl et al.,[7] for the $k_1 k_2^{th}$ LR frame, the image gathering device transforms the continuous input scene $L(x, y)$ into a discrete signal $s_{k_1 k_2}(x, y)$ as defined by:

$$
\begin{aligned}
s_{k_1 k_2}(x, y) &= f_{k_1 k_2}(x, y) \underline{\underline{\text{|||}}}(x, y) \\
&= \left[L(x - x_{k_1}, y - y_{k_2}) * \tau_{k_1 k_2}(x, y) + N_{k_1 k_2}(x, y) \right] \underline{\underline{\text{|||}}}(x, y)
\end{aligned}
\tag{1}
$$

where $\tau(x, y)$ is the spatial response of the image acquisition device, $N_{k_1 k_2}(x, y)$ is the additive photo-detector noise, and the symbol * denotes spatial convolution. The sampling function

$$
\underline{\underline{\text{|||}}}(x, y) = \sum_m \sum_n \delta(x - m, y - n)
\tag{2}
$$

denotes sampling on a rectangular grid with unit sampling intervals and $\delta(x, y)$ is the Dirac delta function. The reconstruction of the output image is performed by interlacing the pixels of the acquired images into a HR grid with a sampling density equals $K_1 K_2$ times the sampling density of the individual LR images. Thus, the composite HR image S is given by:

$$
\tilde{S}(\nu, \omega) = \frac{1}{K_1 K_2} \sum_{k_1=0}^{K_1-1} \sum_{k_2=0}^{K_2-1} \tilde{s}_{k_1 k_2}(\nu, \omega) \exp\left(-i2\pi(\nu\, x_{k_1} + \omega\, y_{k_2})\right)
\tag{3}
$$

we derive the stochastic Wiener filter based on the fully detailed SR CDC model that is given in Figure 1. It is constrained by the periodic and non-periodic inter-relationships between the different frequency components of the proposed SR system. It can be used as reconstruction filter as well as a restoration filter to recover images from the degradations that are introduced during image acquisition and image display. If the number
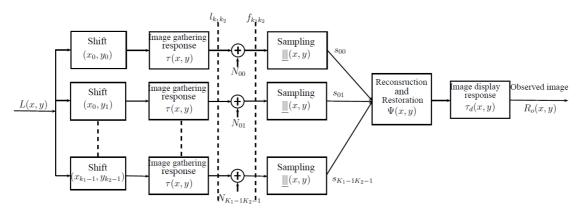
Figure 1: Complete continuous-discrete-continuous SR reconstruction model.

of LR frames is $K_1 K_2$ which is sufficient to produce full SR along the horizontal and vertical dimensions of the reconstructed images then the derived filter works only as a restoration filter. On the other hand, if the available number of LR images is less than $K_1 K_2$, then the filter works as a restoration and a reconstruction filter to estimate missing pixels on the dense HR grid. In spatial domain, the observed image $R_o(x, y)$ is reconstructed through the spatial convolution of the Wiener filter $\Psi(x, y)$, the spatial response of the image display device $\tau_d(x, y)$ and the interlaced image $S(x, y)$ as given by

$$R_o(x, y) = S(x, y) * \Psi(x, y) * \tau_d(x, y) \tag{4}$$

The optimal CDC Wiener restoration filter must satisfy:[2]

$$\frac{\partial e^2}{\partial \hat{\Psi}} = -\hat{\Phi}_{L*S}(\nu, \omega)\hat{\tau}_d(\nu, \omega) + \tilde{\Phi}_S(\nu, \omega)\hat{\Psi}^*(\nu, \omega) \left|\hat{\tau}_d(\nu, \omega)\right|^2$$

$$= 0 \tag{5}$$

Accordingly, the Wiener filter that minimizes the MSRE is given by:

$$\hat{\Psi}(\nu, \omega) = \frac{\hat{\Phi}_{LS*}(\nu, \omega)\hat{\tau}_d^*(\nu, \omega)}{\tilde{\Phi}_S(\nu, \omega) \left|\hat{\tau}_d(\nu, \omega)\right|^2} \tag{6}$$

where the cross power spectrum $\hat{\Phi}_{LS*}(\nu, \omega)$ between the input scene and the reconstructed image is given by:

$$\hat{\Phi}_{LS*}(\nu, \omega) = \frac{1}{K_1 K_2}\hat{\Phi}_L(\nu, \omega) \sum_{k_1 k_2} \hat{\tau}_{k_1 k_2}^*(\nu, \omega) \exp(i4\pi(\nu\, x_{k_1} + \omega\, y_{k_2})) \tag{7}$$

and the power spectrum density of the reconstructed image $\tilde{\Phi}_S(\nu, \omega)$ is given by:

$$\begin{aligned}
\tilde{\Phi}_S(\nu, \omega) &= \frac{1}{K_1^2 K_2^2}\left(\hat{\Phi}_L(\nu, \omega) * \hat{\underline{\underline{|||}}}(\nu, \omega) \sum_{mn} \left|\sum_{k_1 k_2} \left|\hat{\tau}_{k_1 k_2}^*(\nu', \omega')\right|^2 \exp(-i2\pi(\nu'\, x_{k_1} + \omega'\, y_{k_2}))\right|^2 \right.\\
&\quad + \left. \sum_{k_1 k_2} \hat{\Phi}_{N_{k_1 k_2}}(\nu, \omega) * \hat{\underline{\underline{|||}}}(\nu, \omega)\right)
\end{aligned} \tag{8}$$

where $\nu' = 2\nu - m$ and $\omega' = 2\omega - n$. If the photo-detector noise is modeled as wide-sense stationary discrete random process and white, then the Wiener filter can be expressed as a function of the SNR σ_L/σ_N as given by

$$\hat{\Psi}(\nu,\omega) = \frac{K_1 K_2 \hat{\Phi}_L(\nu,\omega)\hat{\tau}^*(\nu,\omega)\hat{\tau}_d^*(\nu,\omega)\exp(i4\pi(\nu x_{k_1}+\omega y_{k_2}))/|\hat{\tau}_d(\nu,\omega)|^2}{\hat{\Phi}_L'(\nu,\omega)*\underline{\underline{|||}}(\nu,\omega)\sum_{mn}\left|\sum_{k_1 k_2}\left|\hat{\tau}_{k_1 k_2}^*(\nu',\omega')\right|^2\exp(-i2\pi(\nu' x_{k_1}+\omega' y_{k_2}))\right|^2 + \sum_{k_1 k_2}(\sigma_L/\sigma_{N_{k_1 k_2}})^{-2}} \tag{9}$$

where $\hat{\Phi}_L'(\nu,\omega) = \sigma_L^{-2}\hat{\Phi}_L(\nu,\omega)$. It can be seen that Wiener filter is a function of the different components of the CDC system, the subpixel shifts of the individual LR frames and the system SNR.

3. ENHANCED CDC MODEL

The registration process has a direct impact on the quality and the performance of any SR algorithm. Inaccurate registration leads to severe results in the reconstructed images. The quality of SR images can be enhanced by adding a parameter that accounts for the registration and fusion errors to the proposed model.[8,9] In our derivation we incorporate new parameters α_{k_1} and β_{k_2} to the SR CDC model to refer to registration and fusion errors. By the appropriate selection of its distribution, Equations (3), (7) and (8) can be re-derived leading to a modified version of Wiener filter. The new equations for the reconstructed image S, the cross power spectrum $\hat{\Phi}_{LS^*}(\nu,\omega)$ and the power spectrum density of the reconstructed image $\tilde{\Phi}_S(\nu,\omega)$ are:

$$
\begin{aligned}
\tilde{S}(\nu,\omega) &= \frac{1}{K_1 K_2}\sum_{k_1=0}^{K_1-1}\sum_{k_2=0}^{K_2-1}\tilde{s}_{k_1 k_2}(\nu,\omega)\\
&\times \exp\left(-i2\pi(\nu(x_{k_1}+\alpha_{k_1})+\omega(y_{k_2}+\beta_{k_2}))\right),
\end{aligned} \tag{10}
$$

$$
\begin{aligned}
\hat{\Phi}_{LS^*}(\nu,\omega) &= \frac{1}{K_1 K_2}\hat{\Phi}_L(\nu,\omega)\sum_{k_1 k_2}\hat{\tau}_{k_1 k_2}^*(\nu,\omega)\exp(i4\pi(\nu x_{k_1}+\omega y_{k_2}))\\
&\times E\left\{\exp i2\pi(\nu(\alpha_{k_1}+\omega(\beta_{k_2}))\right\}
\end{aligned} \tag{11}
$$

and

$$
\begin{aligned}
\tilde{\Phi}_S(\nu,\omega) &= \frac{1}{K_1^2 K_2^2}\left(\hat{\Phi}_L(\nu,\omega)*\underline{\underline{|||}}(\nu,\omega)\sum_{mn}|\sum_{k_1 k_2}\hat{\tau}_{k_1 k_2}^*(\nu',\omega')\exp(-i2\pi(\nu' x_{k_1}+\omega' y_{k_2}))\right.\\
&\times \left. E\left\{\exp i2\pi(\nu\alpha_{k_1}+\omega\beta_{k_2})\right\}|^2 + \sum_{k_1 k_2}\hat{\Phi}_{N_{k_1 k_2}}(\nu,\omega)*\underline{\underline{|||}}(\nu,\omega)\right)
\end{aligned} \tag{12}
$$

respectively, where α_{k_1} and β_{k_2} are the corresponding registration and fusion errors. Farsiu et al.[9] suggested that the registration and fusion errors are properly described by Laplacian distribution. We derived the $E\left\{\exp i2\pi(\nu(\alpha_{k_1}+\omega(\beta_{k_2}))\right\}$ term for three different distributions (Laplacian, uniform , and Gaussian) and compare their performance in terms of the maximum realizable fidelity. If the registration and fusion errors are described by a Laplacian probability density function $f_L(\alpha_{k_1},\beta_{k_2}|b)$ given by

$$f_L(\alpha_{k_1},\beta_{k_2}) = \frac{1}{2b}e^{-\frac{|\alpha_{k_1}|+|\beta_{k_2}|}{b}} \tag{13}$$

where b is a scale parameter and related to the variance of the error then the expectation for the error term is given by

$$
\begin{aligned}
E\left\{e^{i2\pi(\nu\alpha_{k_1}+\omega\beta_{k_2})}\right\} &= \int_{-\infty}^{\infty}e^{i2\pi(\nu\alpha_{k_1}+\omega\beta_{k_2})}f_L(\alpha_{k_1},\beta_{k_2})\,d\alpha_{k_1}d\beta_{k_2}\\
&= \frac{1}{b^2(4\pi^2 b^2\nu^2+1)(4\pi^2 b^2\omega^2+1)}
\end{aligned} \tag{14}
$$

The proposed second distribution is the Gaussian probability function $f_G(\alpha_{k_1}, \beta_{k_2})$ defined by

$$f_G(\alpha_{k_1}, \beta_{k_2}) = \frac{1}{\sqrt{2\pi}\sigma} e^{-\frac{\alpha_{k_1}^2 + \beta_{k_2}^2}{2\sigma^2}} \tag{15}$$

Accordingly, the expectation for the error term is given by

$$
\begin{aligned}
E\left\{e^{i2\pi(\nu\alpha_{k_1} + \omega\beta_{k_2})}\right\} &= \int_{-\infty}^{\infty} e^{i2\pi(\nu\alpha_{k_1} + \omega\beta_{k_2})} f_G(\alpha_{k_1}, \beta_{k_2}) \, d\alpha_{k_1} d\beta_{k_2} \\
&= e^{2\pi^2\sigma^2(\nu^2 + \omega^2)}
\end{aligned}
\tag{16}
$$

Likewise if the the distribution is the uniform probability distribution function $f_U(\alpha_{k_1}, \beta_{k_2})$ defined by

$$
f_U(\alpha_{k_1}, \beta_{k_2}) = \begin{cases} W_x W_y & \text{if } |\alpha_{k_1}| \leq \frac{1}{2W_x}, \ |\beta_{k_y}| \leq \frac{1}{2W_y} \\ 0 & \text{otherwise} \end{cases}
\tag{17}
$$

then the corresponding expectation for the error is given by

$$
\begin{aligned}
E\left\{e^{i2\pi(\nu\alpha_{k_1} + \omega\beta_{k_2})}\right\} &= \int_{-\infty}^{\infty} e^{i2\pi(\nu\alpha_{k_1} + \omega\beta_{k_2})} f_U(\alpha_{k_1}, \beta_{k_2}) \, d\alpha_{k_1} d\beta_{k_2} \\
&= \text{sinc}(\frac{\nu}{W_x})\text{sinc}(\frac{\omega}{W_y})
\end{aligned}
\tag{18}
$$

4. SPEEDED-UP WIENER FILTER

The main drawback of the proposed SR reconstruction and restoration Wiener filter is its computational time required to prepare the Wiener filter in the frequency domain using Equation (9). The idea here is to reduce the dimensions of the Wiener filter by constraining it to work on small patches on the images. As a result the required time to prepare the filter is reduced in addition to the time required to apply fast Fourier transform and its inverse operations. Back to Equation (4), the interlaced image $S(x, y)$ can be expanded as

$$
S(x, y) = \begin{bmatrix} P_{11} & \mathbf{0} & \dots & \mathbf{0} \\ \mathbf{0} & \mathbf{0} & \dots & \mathbf{0} \\ \vdots & \vdots & \vdots & \vdots \\ \mathbf{0} & \mathbf{0} & \dots & \mathbf{0} \end{bmatrix} + \begin{bmatrix} \mathbf{0} & P_{12} & \dots & \mathbf{0} \\ \mathbf{0} & \mathbf{0} & \dots & \mathbf{0} \\ \vdots & \vdots & \vdots & \vdots \\ \mathbf{0} & \mathbf{0} & \dots & \mathbf{0} \end{bmatrix} + \dots \begin{bmatrix} \mathbf{0} & \mathbf{0} & \dots & \mathbf{0} \\ \mathbf{0} & \mathbf{0} & \dots & \mathbf{0} \\ \vdots & \vdots & \vdots & \vdots \\ \mathbf{0} & \mathbf{0} & \dots & P_{p_1 p_2} \end{bmatrix}
\tag{19}
$$

where P_{ij} represents the ij^{th} partition, $\mathbf{0}$ is a block zero matrix of dimension $L_1 \times L_2$ and p_1 and p_2 are the number of partition in the $x-$ and $y-$ directions respectively. Suppose that $S(x, y)$ and $P_{ij}(x, y)$ are of dimension $M_1 \times M_2$ and $L_1 \times L_2$ respectively, then P_{ij} can be written as

$$P_{ij} = S(iL_1 : (i + 1)L_1 - 1, jL_2 : (j + 1)L_2 - 1) \tag{20}$$

As a result of this partitioning, Wiener filter can be applied independently to each of these partitions and because they are dominated by zeros in a well organized structure it can be applied efficiently to its nonzero part. The size of the derived Wiener filter can be constrained to the size of the P_{ij} matrix and as a consequence its performance is expected to improve. The main parameters that control the derivation of the Wiener filter are the subpixel shifts of LR images and the mean spatial detail of the acquired scene. After the subpixel shift adjustments, these subpixel shifts constitute a uniform structure and are the same for all partitions. Also, as a good approximation of the mean spatial detail of the scene can be taken as the average spatial detail across all the partition. As a consequence, only one Wiener filter can be used efficiently in the reconstruction and restoration of all partitions which enables parallelization of the process and reduces the total time required for the processing of the whole image. Figure 2 shows the pipeline for the implementation of the speeded-up Wiener filter. It can be prepared in the frequency domain with the new smaller dimension and then it's pointwise multiplied with Fourier transform of every partition. Every partition will be recovered independently by means of inverse Fourier transform and finally all the processed partitions can be combined again to construct the final reconstructed SR image. If $M_1 = M_2 = M$ and $L_1 = L_2 = L$, then the new computational complexity of the processing of the Fourier transform operations is $L \log_2 L$ compared to $M \log_2 M$ for the older one.
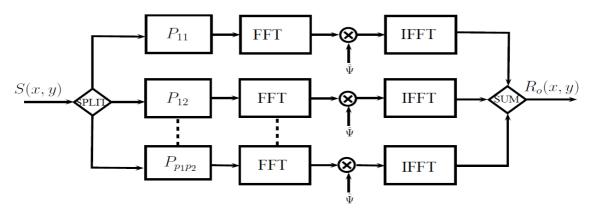
Figure 2: Pipeline of the speeded Up Wiener filter.

5. INFORMATION THEORETIC APPROACH FOR SR VISUAL QUALITY ASSESSMENT

In this section we incorporate the information theory into the visual quality assessment of the reconstructed SR images. We emphasize on the close correlation between the information rate and the visual quality of the images. The higher the information rate the better the visual quality. The proposed model contains two major transformations: (i) the continuous-to-discrete transformation of the continuous input image $L(x,y)$ into discrete interlaced image $S(x,y)$ and (ii) the digital-to-continuous transformation of the discrete interlaced image $S(x,y)$ into the continuous output image $R_o(x,y)$. We propose two figures of merits: (i) information rate $\mathcal{H}$ and (ii) maximum realizable fidelity $\mathcal{F}$ that can be used to assess these transformations. The information rate assess the first transformation while the maximum realizable fidelity assess the end-to-end CDC transformation. In addition, the information rate is used to measure the amount of information that the image gathering device is producing while the maximum realizable fidelity is used to compare the closeness between the reconstructed restored output images and the original input HR scenes.

5.1 Information rate

Shannon[10, 11] defined the information rate that is produced by the image acquisition device or in other words the mutual information between the continuous input scene L and the discrete interlaced image S as

$$\mathcal{H} = \mathcal{E}[S(x,y)] - \mathcal{E}[S(x,y)|L(x,y)] \tag{21a}$$

$$\mathcal{H} = \mathcal{E}[\tilde{S}(\nu,\omega)] - \mathcal{E}[\tilde{S}(\nu,\omega)|\hat{L}(\nu,\omega)] \tag{21b}$$

where $\mathcal{E}[\cdot]$ refers to the entropy of the interlaced image $S(x,y)$ defined in the spatial and frequency domains, respectively, and the , $\mathcal{E}[\cdot|\cdot]$, is the conditional entropy of the same interlaced image given the input scene. The composite image $\tilde{S}(\nu,\omega)$ in Equation (3) can be rewritten as

$$\tilde{S}(\nu,\omega) = \frac{1}{K_1 K_2} \sum_{k_1 k_2} \hat{L}(\nu,\omega)\hat{\tau}_{k_1 k_2}(\nu,\omega) \exp(-i4\pi(x_{k_1}\nu + y_{k_2}\omega)) + \hat{n}(\nu,\omega) \tag{22}$$

where $\hat{n}(\nu,\omega)$ represents the composite noise that results from aliasing and the photodetector noise and it is given by

$$\hat{n}(\nu,\omega) = \frac{1}{K_1 K_2} \sum_{k_1 k_2} \left[\hat{N}_a(\nu,\omega) + \tilde{N}_{k_1 k_2}(\nu,\omega) \right] \exp(-i2\pi(x_{k_1}\nu + y_{k_2}\omega)) \tag{23}$$

If the aliased noise components and the photo-detector noise are assumed to be independent additive Gaussian noise, then the information rate can be simplified to[11]

$$\mathcal{H} = \mathcal{E}[S(x,y)] - \mathcal{E}[n(x,y)] \tag{24a}$$

$$\mathcal{H} = \mathcal{E}[\tilde{S}(\nu,\omega)] - \mathcal{E}[\hat{n}(\nu,\omega)] \tag{24b}$$

Equation (24a) measures the mutual information between the input scene and the interlaced image $S(x,y)$. Thus it gives the obtainable amount of information of the image gathering device minus the noise component. If the Gaussian probability density $P_S[\tilde{S}(\nu,\omega)]$ of the composite image $\tilde{S}(\nu,\omega)$ and the Gaussian probability $P_n[\hat{n}(\nu,\omega)]$ of the noise are given by

$$P_S[\tilde{S}(\nu,\omega)] = \frac{1}{\pi\tilde{\Phi}_S(\nu,\omega)} \exp\left[-\left|\tilde{S}(\nu,\omega)\right|^2 / \tilde{\Phi}_S(\nu,\omega)\right] \tag{25}$$

and

$$P_n[\hat{n}(\nu,\omega)] = \frac{1}{\pi\hat{\Phi}_n(\nu,\omega)} \exp\left[-|\hat{n}(\nu,\omega)|^2 / \hat{\Phi}_n(\nu,\omega)\right] \tag{26}$$

respectively, then the information rate $\mathcal{H}$ can be written as[12]

$$
\begin{aligned}
\mathcal{H} &= \frac{1}{2} \iint_{\hat{B}} \log_2 \frac{\tilde{\Phi}_S(\nu,\omega)}{\hat{\Phi}_n(\nu,\omega)}\, d\nu d\omega \\
&= -\frac{1}{2} \iint_{\hat{B}} \log_2 \frac{\hat{\Phi}_n(\nu,\omega)}{\tilde{\Phi}_S(\nu,\omega)}\, d\nu d\omega
\end{aligned}
\tag{27}
$$

where the PSD $\tilde{\Phi}_S(\nu,\omega)$ is given by

$$
\begin{aligned}
\tilde{\Phi}_S(\nu,\omega) = {} & \frac{1}{K_1^2 K_2^2} \Bigg[\hat{\Phi}_L(\nu,\omega) * \underline{\underline{\text{III}}}(\nu,\omega) \sum_{mn} \Bigg| \sum_{k_1 k_2} \hat{\tau}_{k_1 k_2}(\nu - m, \omega - n) \\
& \times\ \exp(-i2\pi((2\nu - m)x_{k_1} + (2\omega - n)y_{k_2})) \Bigg|^2 \\
& +\ \sum_{k_1 k_2} \hat{\Phi}_{k_1 k_2}(\nu,\omega) * \underline{\underline{\text{III}}}(\nu,\omega) \Bigg]
\end{aligned}
\tag{28}
$$

and the PSD $\hat{\Phi}_n(\nu,\omega)$ is given by

$$
\begin{aligned}
\tilde{\Phi}_n(\nu,\omega) = {} & \frac{1}{K_1^2 K_2^2} \Bigg[\hat{\Phi}_L(\nu,\omega) * \underline{\underline{\text{III}}}_s(\nu,\omega) \sum_{mn} \Bigg| \sum_{k_1 k_2} \hat{\tau}_{k_1 k_2}(\nu - m, \omega - n) \\
& \times\ \exp(-i2\pi((2\nu - m)x_{k_1} + (2\omega - n)y_{k_2})) \Bigg|^2 \\
& +\ \sum_{k_1 k_2} \hat{\Phi}_{k_1 k_2}(\nu,\omega) * \underline{\underline{\text{III}}}(\nu,\omega) \Bigg]
\end{aligned}
\tag{29}
$$

Accordingly, $\tilde{\Phi}_S(\nu,\omega)$ can be written as

$$
\begin{aligned}
\tilde{\Phi}_S(\nu,\omega) = {} & \hat{\Phi}_n(\nu,\omega) + \frac{1}{K_1^2 K_2^2} \hat{\Phi}_L(\nu,\omega) \Bigg| \sum_{k_1 k_2} \hat{\tau}_{k_1 k_2}(\nu,\omega) \\
& \times\ \exp(-i4\pi(\nu x_{k_1} + \omega y_{k_2})) \Bigg|^2
\end{aligned}
\tag{30}
$$

By using Equation (29) and (30) into Equation (27), the information rate $\mathcal{H}$ can be written as

$$
\begin{aligned}
\mathcal{H} = & -\frac{1}{2} \iint_{\hat{B}} \log_2 \left[1 - \frac{1}{K_1^2 K_2^2} \frac{\hat{\Phi}_L(\nu,\omega)}{\hat{\Phi}_S(\nu,\omega)} \left| \sum_{k_1 k_2} \hat{\tau}_{k_1 k_2}(\nu,\omega) \right. \right. \\
& \times \left. \left. \exp(-i4\pi(\nu x_{k_1} + \omega y_{k_2})) \right|^2 \right]
\end{aligned}
\tag{31}
$$

From Equation (6), $\tilde{\Phi}_S(\nu,\omega)$ can be written as

$$
\tilde{\Phi}_S(\nu,\omega) = \frac{1}{K_1 K_2} \frac{\hat{\Phi}_L(\nu,\omega)}{\hat{\Psi}(\nu,\omega)} \sum_{k_1 k_2} \hat{\tau}^*_{k_1 k_2}(\nu,\omega) \exp(i4\pi(\nu x_{k_1} + \omega y_{k_2}))
\tag{32}
$$

Substituting Equation (32) into Equation (31) yields

$$
\mathcal{H} = -\frac{1}{2} \iint_{\hat{B}} \log_2 \left[1 - \frac{\hat{\Psi}(\nu,\omega)}{K_1 K_2} \sum_{k_1 k_2} \hat{\tau}_{k_1 k_2}(\nu,\omega) \exp(-i4\pi(\nu x_{k_1} + \omega y_{k_2})) \right]
\tag{33}
$$

Thus, the information rate produced by the imaging gathering device depends on its optical response index, the design of Wiener filter, and the inter-subpixel shifts between the individual LR frames. From Equation (6), the minimum MSRE error $\hat{\epsilon}^2_{\min}(\nu,\omega)$ can be expressed as

$$
\hat{\epsilon}^2_{\min}(\nu,\omega) = \hat{\Phi}_L(\nu,\omega) \left(1 - \hat{\Gamma}(\nu,\omega) \right)
\tag{34}
$$

where $\hat{\Gamma}$ is given by

$$
\hat{\Gamma}(\nu,\omega) = \frac{\hat{\Psi}(\nu,\omega)}{K_1 K_2} \sum_{k_1 k_2} \hat{\tau}_{k_1 k_2}(\nu,\omega) \exp\left(i4\pi \left(x_{k_1} \nu + y_{k_2} \omega \right) \right)
\tag{35}
$$

By comparing Equations (33), (34) and (35), the information rate can be written as

$$
\mathcal{H} = -\frac{1}{2} \iint_{\hat{B}} \log_2 \left[1 - \hat{\Gamma}(\nu,\omega) \right] d\nu d\omega
\tag{36a}
$$

$$
\mathcal{H} = \frac{1}{2} \iint_{\hat{B}} \log_2 \frac{\hat{\Phi}_L(\nu,\omega)}{\hat{\epsilon}^2_{\min}} d\nu d\omega
\tag{36b}
$$

$$
\mathcal{H} = \frac{1}{2} \iint_{\hat{B}} \log_2 \hat{\Phi}_L(\nu,\omega) \, d\nu d\omega - \frac{1}{2} \iint_{\hat{B}} \log_2 \hat{\epsilon}^2_{\min} \, d\nu d\omega
\tag{36c}
$$

The first term in Equation (36c) represents the information rate that the image gathering device can produce without any degradations during the acquisition process and the second term refers to the loss in the information rate caused by the CDC system degradations.

5.2 Maximum realizable fidelity

Linefoot[13] defined the fidelity the similarity between the continuous input scene and the reconstructed output scene as given by

$$
\mathbf{F} = 1 - \sigma_L^{-2} \iint \hat{\epsilon}^2(\nu,\omega) \, d\nu d\omega
\tag{37}
$$

By substituting the minimum MSRE cost function given by Equation (34) into Equation (37), the maximum realizable fidelity $\mathcal{F}$ is given by

$$
\mathcal{F} = \sigma_L^{-2} \iint \hat{\Phi}_L(\nu,\omega) \hat{\Gamma}(\nu,\omega) \, d\nu d\omega
\tag{38}
$$

From Equation (36), the information rate spectral distribution $\hat{\mathcal{H}}(\nu, \omega)$ is given by

$$\hat{\mathcal{H}}(\nu, \omega) = -\log_2 \left[1 - \hat{\Gamma}(\nu, \omega) \right] \tag{39}$$

Accordingly the maximum realizable fidelity $\mathcal{F}$ is given by

$$\mathcal{F} = \sigma_L^{-2} \iint \hat{\Phi}_L(\nu, \omega) \left[1 - 2^{-\hat{\mathcal{H}}(\nu, \omega)} \right] d\nu d\omega \tag{40}$$

It can be concluded that whenever the information rate spectral distribution $\hat{\mathcal{H}}(\nu, \omega)$ is high over all the spectrum then $\mathcal{F}$ hits its maximum value for a given image gathering device.

6. SIMULATIONS AND RESULTS

To assess and evaluate the proposed approach, we used the random polygons image shown in Figure 3 to simulate and analyze the Weiner restoration filter results. The random polygon consists of regions whose boundaries are distributed according to Poisson probability with a mean separation μ and whose input scene magnitudes are distributed according to independent zero-mean Gaussian statistics of variance σ_L^2. The mean separation μ is measured relative to the sampling interval of the image-gathering device and treated as the mean spatial detail of the scene.[3] In our simulations, we started with a simulated high resolution scene that is blurred by a Gaussian
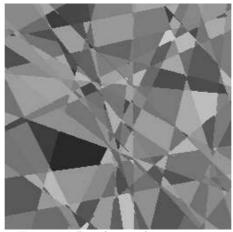

Figure 3: Random polygon image.

low-pass filter defined as:

$$\hat{\tau}(\nu, \omega) = \exp \left[-\frac{\nu^2 + \omega^2}{\sigma^2} \right] \tag{41}$$

where σ is the optical-response index for which $\hat{\tau}(\nu, \omega) \approx 0.37$. This Gaussian filter approximates the SFR of the image-gathering device. Schade[14] and Schreiber[15] concluded that the image-gathering device with SFR $\hat{\tau}(\nu, \omega)$ characterized by $\sigma = 0.8$ provides generally the most favorable trade-off between sharpness and aliasing artifacts without the aid of digital processing. The simulated HR images are down sampled by a factor of 2 and white noise and blurring are superimposed to them such that the blurred signal-to-noise ratio (BSNR) is 30 dB:

$$\text{BSNR} = 10 \log_{10} \left(\frac{\sigma_L^2}{\sigma_N^2} \right) \tag{42}$$

where σ_L^2 is the variance of the blurred image scene and σ_N^2 is the variance of the white noise. The derivation of the Weiner restoration filter depends on the estimation of the input scene PSD $\hat{\Phi}_L$. Itakura et al.[16] have shown that the PSD of natural scenes can be approximated by:

$$\hat{\Phi}_L(\nu, \omega) = \frac{2\pi \mu^2 \sigma_L^2}{\left[1 + (2\pi\mu\rho)^2 \right]^{3/2}}, \tag{43}$$

where $\rho^2 = \nu^2 + \omega^2$ and μ is the scene mean spatial detail. The HR image is reconstructed and Weiner filter is applied to restore the images from the degradations encountered in the image-gathering process. The fidelity
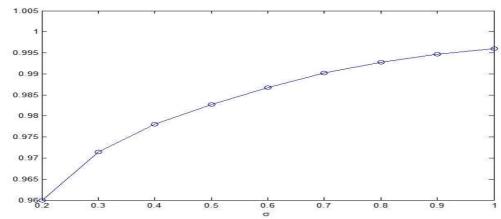

Figure 4: Fidelity between simulated HR scene and the reconstructed images for different image-gathering optical response index (σ).

is used as comparison metric between the original HR image and the reconstructed one. Figure 4 shows the fidelity between the simulated HR images and the reconstructed ones. The greater the optical-response index σ of the image-gathering device the better the fidelity between the reconstructed and the simulated HR scenes. Figure 5 shows a comparison between the realizable fidelity for the enhanced CDC model. It can be seen that the maximum realizable fidelity is achieved when the registration and fusion errors are described by Laplacian model which is similar to the assumption proposed by Farsiu et al.[9] Also, if the error is modeled by Gaussian, it is still have a higher fidelity compared to the cases of using the model without the new error parameter or using the uniform probability model. In our simulations and to assess the close correlation between the visual
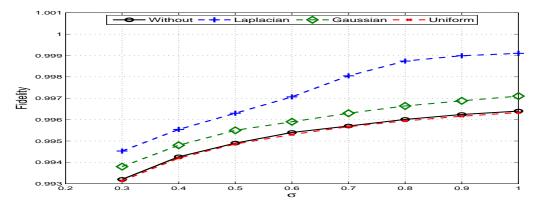

Figure 5: Fidelity comparison for different registration and fusion models with different image-gathering optical index σ.

quality and both the information rate and the maximum realizable fidelity, we discussed three cases: (a) for a given MSD and SNR of 3 and 32 respectively, we compared the change in the information rate with the optical response index σ that controls the design of the image gathering device; (b) Similar to the first case, we compared the change in the information rate with the total SNR of the system when σ is 0.8 and for a given input scene with MSD of 3; (c) finally, we discussed the change in the information rate with the MSD of the input scenes while keeping both the SNR at 32 and for a given image gathering device with optical response index of $\sigma = 0.8$. Figure 6, 7, and 8 show the results of these three cases. The information rate produced by the image gathering device improves with the increase in its spatial response index that controls the trade off between the aliasing and blur and also it improves with the enhancement in the system SNR that reflects the reduction in the effect

of the total noise in the system. Also, the amount of information produced by the image device is affected with the mean spatial detail of the scene. The smaller the MSD the higher the information contained in the output scene.
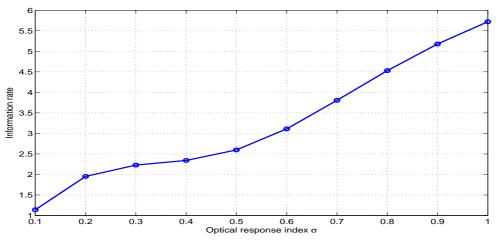

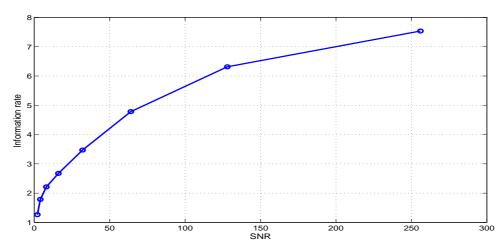Figure 6: Information rate comparison against optical response index σ.

Figure 7: Information rate comparison against SNR.

The computational costs of the different SR techniques are listed in Table 1. The simulations are performed using MATLAB 7.8 Release 2009a program on OPTIPLEX 780 (Intel(R) Core (TM)2 Quad 2.66 GHz CPU, 8.00 GB RAM, MS Windows 7 Professional 2009). We compared the performance of our method with some of the well-known SR reconstruction approaches in terms of fidelity, visual quality assessment and the computational time. These techniques are non-uniform interpolation, Papoulis-Gerchberg,[17] iterated back projection,[18] roubust SR,[19] POCS[20] and structure-adaptive normalized convolution.[21] All of these algorithms were developed at the Laboratory of Audiovisual Communications (LCAV), Ecole Polytechnique Federale de Lausanne (EPFL), Switzerland.[22] It can be seen from Table 1 that Wiener computational time is much smaller than the other SR techniques. Most of Wiener computational time is consumed in a preprocessing step (0.355 s in case of partial SR and 0.78 s in case of full SR) which is considered as the main demerit of this approach. The results of the speeded-up Wiener filter are shown in Table 2. As can be seen from the results, we enhanced the performance of the filter in terms of its speed and it's faster than the original one. Also, by increasing the number of partitions
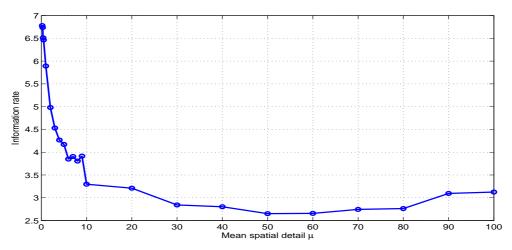
Figure 8: Information rate comparison against mean spatial detail μ.

we can parallelize the process and reduce both the computational time and memory requirements.

Table 1: Computational time for reconstructed SR images (s).

SR Techniques	Stochastic Wiener	Non-Uniform interpolation	Robust SR	POCS	Adaptive convolution	Iterative back projection
Computational Time	0.92	2.839	36.56	13.665	11.716	13.713

Table 2: Improvements in computational time using speeded-up Wiener filter (s).

SR Techniques	Normal Wiener	Wiener with 4 partitions	Wiener with 16 partitions
Computational Time	0.92	0.3978	0.1326

7. CONCLUSIONS

In this paper we propose a new fast enhanced Wiener filter for SR reconstruction and restoration that is basically depend on the fully detailed SR CDC model depicted in Figure 1. This filter is used to boost the visual quality of the SR image that is affected by degradations during the acquisition such as blur due to system optics, aliasing due to insufficient sampling, photodetector noise, registration and fusion error, the number of scenels, and their relative arrangement on the high resolution grid. We introduced its mathematical derivation and analyze the end-to-end model and formulated the Wiener filter as a function of the parameters associated with the proposed SR system such as image gathering and image display response indices, system average signal-to-noise ratio (SNR) and inter-subpixel shifts between the LR images. In addition, we added a new parameter that accounts for LR images registration and fusion errors in order to improve the overall system performance. Also, we speeded-up the filter performance by constraining it to work on small patches of the images and consequently it can be implemented efficiently in the frequency domain. Also, we analyzed the loss in the end-to-end system

fidelity and separated into three components and every component is related to its corresponding degradation in the proposed system which enables a good design of the SR model. In addition, we proposed two figures of merit: The information rate and the maximum realizable fidelity. Both are based on the information theory to asses the visual quality of the reconstructed images. The information rate is used to measure the amount of information produced by the imaging gathering device while the maximum realizable fidelity is used to measure the closeness between the reconstructed output and the original HR scene. It is shown that SR images can be reconstructed with both high information rate and maximum realizable fidelity.